Supporting Information for: The Impact of Metal Centers in the M-MOF-74 Series on Carbon Dioxide and Hydrogen Separation

Dominika O. Wasik,[†,‡] José Manuel Vicent-Luna,[*,†] Azahara Luna-Triguero,[¶,‡] David Dubbeldam,[§] Thijs J. H. Vlugt,[‖] and Sofía Calero[*,†,‡]

†*Materials Simulation and Modelling, Department of Applied Physics, Eindhoven University of Technology, 5600MB Eindhoven, The Netherlands*

‡*Eindhoven Institute for Renewable Energy Systems, Eindhoven University of Technology, PO Box 513, Eindhoven 5600 MB, The Netherlands*

¶*Energy Technology, Department of Mechanical Engineering, Eindhoven University of Technology, 5600MB Eindhoven, The Netherlands*

§*Van't Hoff Institute for Molecular Sciences, University of Amsterdam, 1098XH Amsterdam, The Netherlands*

‖*Engineering Thermodynamics, Process & Energy Department, Faculty of Mechanical, Maritime and Materials Engineering, Delft University of Technology, Leeghwaterstraat 39, Delft 2628CB, The Netherlands*

E-mail: j.vicent.luna@tue.nl; s.calero@tue.nl

- Cell parameters for M-MOF-74 (M = Ni, Cu, Co, Fe, Mn, Zn);
- Lennard-Jones and Coulombic interaction potentials for CO_2, H_2 and M-MOF-74 frameworks;
- Parameters of the dual-site Langmuir-Freundlich model for CO_2 and H_2, obtained from RUPTURA;
- Adsorption isotherms of H_2 in M-MOF-74 (M = Ni, Cu, Co, Fe, Mn, Zn), and the corresponding enthalpy of adsorption obtained from grand-canonical Monte Carlo simulations at 77 K and 10^{-5} - 10^{2} kPa;
- Henry coefficients computed from the adjusted force field using Widom's test particle insertions at 77 K, compared to the coefficients calculated from the slope of experimental isotherms in the linear region at low pressures;
- Adsorption isotherms of H_2 in M-MOF-74 (M = Ni, Cu, Co, Fe, Mn, Zn) obtained from grand-canonical Monte Carlo simulations at 87 K and 10^{-5} - 10^{2} kPa;
- Distribution of the CO_2, and H_2 molecules inside M-MOF-74 (M = Co, Fe, Mn, Zn) analyzed using density profiles from grand-canonical Monte Carlo simulations at 298 K, 100 kPa;
- Comparison of breakthrough curves of CO_2/H_2 mixtures at y_{CO_2} = 0.1, 0.2, 0.3, 0.4, 0.5, 0.9 for M-MOF-74, where M = Co, Fe, Mn, Zn;
- Comparison of breakthrough curves of CO_2/H_2 mixtures in M-MOF-74 (M = Ni, Cu, Co, Fe, Mn, Zn) for y_{CO_2} = 0.1, 0.9;
- Prediction of adsorption of CO_2/H_2 mixtures at y_{CO_2} = 0.5 in M-MOF-74 (M = Ni, Cu, Co, Fe, Mn, Zn) using Ideal Adsorption Solution Theory;
- Detailed information on the M-MOF-74 (M = Ni, Cu, Co, Fe, Mn, Zn) structures in the form of cif files.

Table S1: Cell parameters for M-MOF-74 (M = Ni, Cu, Co, Fe, Mn, Zn) obtained from experimental synthesis.[1–6]

MOF-74	a/[Å]	b/[Å]	c/[Å]	α/[°]	β/[°]	γ/[°]	V/[Å^3]
Ni-	25.7856	25.7856	6.7701	90	90	120	15593.4
Cu-	25.9972	25.9972	6.2587	90	90	120	14653
Co-	25.885	25.885	6.8058	90	90	120	15796.7
Fe-	26.1627	26.1627	6.8422	90	90	120	16223.8
Mn-	25.7824	25.7824	6.9126	90	90	120	15917.6
Zn-	25.9322	25.9322	6.8365	90	90	120	15925.9

Table S2: Lennard-Jones and Coulombic interaction potentials for M-MOF-74 (M = Ni, Cu, Co, Fe, Mn, Zn) frameworks,[7,8] CO_2,[9,10] and H_2.[11] It is important to note that there is an exception/override to the use of the Lorentz-Berthelot mixing rules[12] for H_{com}–Me interactions. The listed charges for M-MOF-74 atoms were obtained by scaling initial charges computed using the 'charge-equilibration' method of Wilmer and Snurr[13,14] by a factor within the range of 0.5 - 1.5. The set of charges leading to the closest results to the experimental uptakes and the enthalpies of CO_2 adsorption[15] was selected for further study as a part of the final force field. All the frameworks and molecules are charge-neutral. The schematic representation of M-MOF-74 series with the atoms labelled is visualized in Figure 1 of the manuscript. The charges for Co- and Fe-MOF-74 for CO_2 adsorption have been previously published by Luna-Triguero et al.[16]

Atom	ϵ/k_B /[K]	σ /[Å]	q /[e$^-$]
O_{CO_2}	85.671	3.017	-0.3256
C_{CO_2}	29.93	2.742	0.6512
H_{com}	36.7	2.958	-0.936
H_{H_2}	0	0	0.468
	Ni-MOF-74		
Ni	7.556	2.525	1.55
C1	47.86	3.473	0.603
C2	47.86	3.473	-0.275
C3	47.86	3.473	0.275
C4	47.86	3.473	-0.086
O1	48.19	3.0331	-0.63
O2	48.19	3.0331	-0.815
O3	48.19	3.0331	-0.702
H	7.65	2.8464	0.08
	Cu-MOF-74		
Cu	2.518	3.114	0.834
C1	47.86	3.473	-0.076
C2	47.86	3.473	0.345
C3	47.86	3.473	0.156
C4	47.86	3.473	-0.139
O1	48.19	3.0331	-0.394
O2	48.19	3.0331	-0.431
O3	48.19	3.0331	-0.368
H	7.65	2.8464	0.073

Co-MOF-74			
Co	7.052	2.559	1.335
C1	47.86	3.473	0.485
C2	47.86	3.473	-0.207
C3	47.86	3.473	0.245
C4	47.86	3.473	-0.125
O1	48.19	3.0331	-0.544
O2	48.19	3.0331	-0.611
O3	48.19	3.0331	-0.673
H	7.65	2.8464	0.095
Fe-MOF-74			
Fe	6.542	2.594	1.226
C1	47.86	3.473	0.356
C2	47.86	3.473	-0.148
C3	47.86	3.473	0.175
C4	47.86	3.473	-0.088
O1	48.19	3.0331	-0.602
O2	48.19	3.0331	-0.439
O3	48.19	3.0331	-0.561
H	7.65	2.8464	0.081
Mn-MOF-74			
Mn	6.549	2.638	1.161
C1	47.86	3.473	0.368
C2	47.86	3.473	-0.175
C3	47.86	3.473	0.175
C4	47.86	3.473	-0.064
O1	48.19	3.0331	-0.548
O2	48.19	3.0331	-0.443
O3	48.19	3.0331	-0.522
H	7.65	2.8464	0.048
Zn-MOF-74			
Zn	62.3992	2.461	1.006
C1	47.86	3.473	0.343
C2	47.86	3.473	-0.155

C3	47.86	3.473	0.161
C4	47.86	3.473	-0.083
O1	48.19	3.0331	-0.479
O2	48.19	3.0331	-0.393
O3	48.19	3.0331	-0.464
H	7.65	2.8464	0.064
	overrides		
H_{com} - Ni	216.4823	2.1932	
H_{com} - Cu	11.5357	3.036	
H_{com} - Co	17.6963	2.2068	
H_{com} - Fe	18.5939	2.776	
H_{com} - Mn	13.9529	2.798	
H_{com} - Zn	43.069	2.7095	

Table S3: Parameters of the dual-site Langmuir-Freundlich model[17] obtained from fitting on adsorption isotherms data of pure CO_2 and H_2 in M-MOF-74 (M = Ni, Cu, Co, Fe, Mn, Zn) frameworks, computed using the RASPA software package.[18,19] The fitting was performed by RUPTURA[20] and the resulted model parameters were used as an input for breakthrough simulations. The functional form of the dual-site Langmuir-Freundlich isotherm model[17] is expressed as:

$$q(p) = \sum_i q_i^{\text{sat}} \frac{b_i (\frac{p_i}{p_0})^{v_i}}{1 + b_i (\frac{p_i}{p_0})^{v_i}} \tag{1}$$

where $q(p)$ is absolute loading of the adsorbed phase as a function of pressure, q_i^{sat} is saturation loading, b_i is the coefficient of adsorption representing the affinity of the molecule, v_i is heterogeneity factor, p_i is the partial pressure in the gas phase in units of Pa, p_0 is the reference pressure equal to 1 Pa, and i refers to component i.

MOF-74	adsorbate	q_1^{sat} [mol (kg framework)$^{-1}$]	b_1 [-]	v_1 [-]	q_2^{sat} [mol (kg framework)$^{-1}$]	b_2 [-]	v_2 [-]
Ni-	CO_2	12.0936	0.228134	0.0938348	7.10943	$2.13 \cdot 10^{-5}$	0.891086
	H_2	2	$1.36 \cdot 10^{-12}$	1.76051	1.99999	$7.58 \cdot 10^{-8}$	1.09375
Cu-	CO_2	8.04687	0.00780695	0.336492	5.46875	$2.41 \cdot 10^{-10}$	1.79974
	H_2	2.19767	$2.18 \cdot 10^{-11}$	1.60905	1.57042	0.000166379	0.475571
Co-	CO_2	4.3995	0.0557628	0.321359	9.41687	$9.63 \cdot 10^{-5}$	0.783058
	H_2	1.94147	$1.58 \cdot 10^{-8}$	1.17914	1.79365	$3.30 \cdot 10^{-10}$	1.39858
Fe-	CO_2	15.4219	0.0043923	0.468742	0.124994	$4.34 \cdot 10^{-10}$	1.73161
	H_2	2	$4.48 \cdot 10^{-10}$	1.39075	1.12567	$2.94 \cdot 10^{-10}$	1.49625
Mn-	CO_2	11.75	0.0031686	0.524252	2.12503	$3.54 \cdot 10^{-10}$	1.72654
	H_2	2	$5.80 \cdot 10^{-11}$	1.54346	1.5	$4.59 \cdot 10^{-7}$	0.941039
Zn-	CO_2	5.82052	$1.06 \cdot 10^{-5}$	0.939475	6.65485	0.00131705	0.628489
	H_2	1.31477	$4.17 \cdot 10^{-10}$	1.47217	1.96875	$2.56 \cdot 10^{-10}$	1.40625

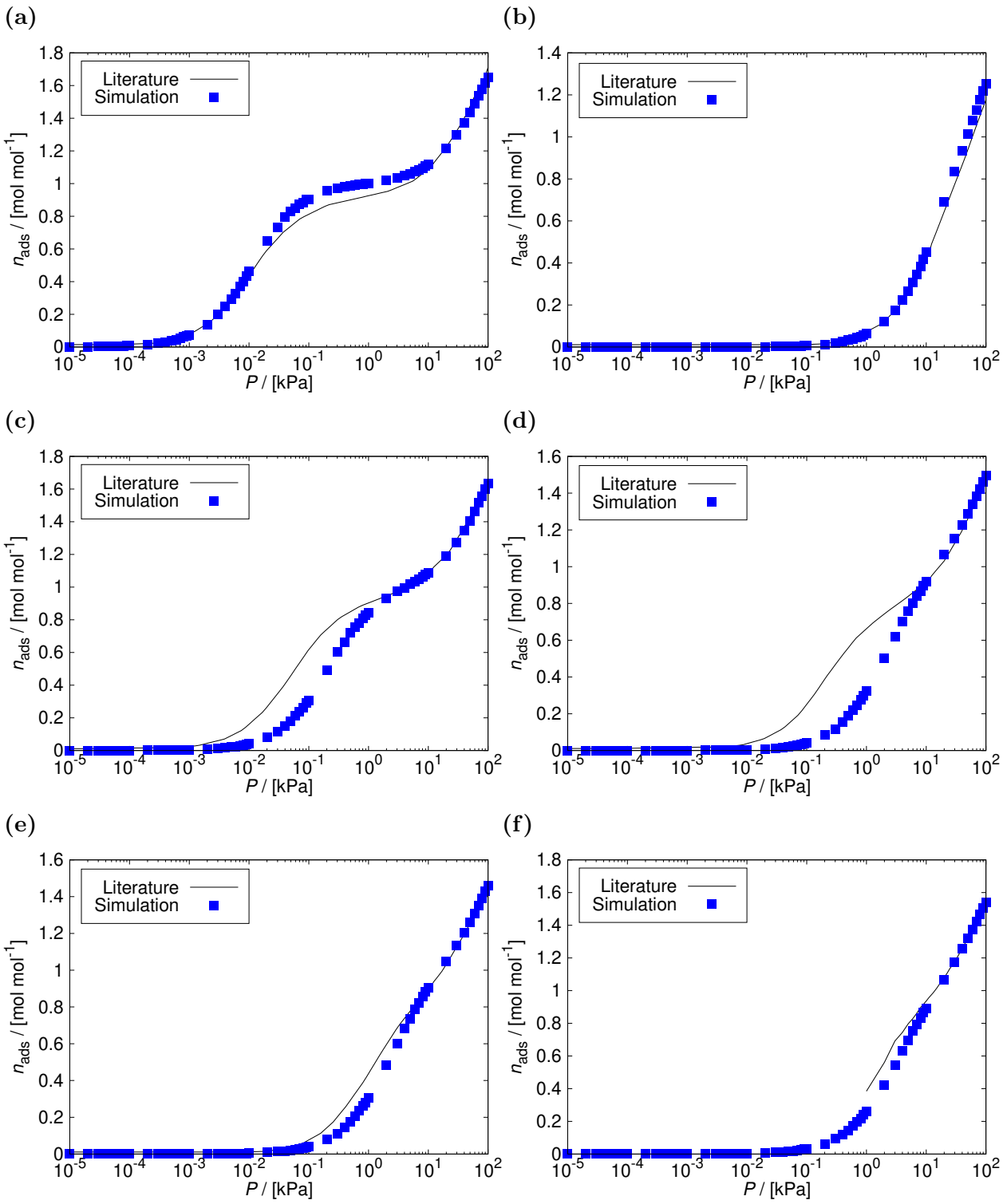

Fig. S1. Adsorption isotherms of H_2 computed from GCMC simulations using the RASPA software package[18,19] at 77 K, and 10^{-5} - 10^{2} kPa in: (a) Ni-MOF-74, (b) Cu-MOF-74, (c) Co-MOF-74, (d) Fe-MOF-74, (e) Mn-MOF-74, and (f) Zn-MOF-74. The adsorption results computed from the adjusted force field are represented by blue data points, and the experimental data from literature[21] by solid black lines. The error bars are smaller than the size of the symbols. The force field agrees well with the experimental values, exhibiting considerable deviation only for Fe-MOF-74 at low pressure range.

Table S4: Henry coefficients for adsorption of H_2 in M-MOF-74 (M = Co, Fe, Mn, Zn) computed from the adjusted force field using Widom's test particle insertions[22] at 77 K, and calculated from the slope of experimental isotherms[21] in the linear region at low pressures by:[23]

$$q = K_{\mathrm{H}} \cdot P \tag{2}$$

where q is the adsorption loading of H_2 in M-MOF-74, K_{H} is the Henry coefficient, and P is the pressure. The experimental adsorption data for Zn-MOF-74 is not available at the Henry regime. The Henry coefficients for Cu-MOF-74 and Ni-MOF-74 were computed with high accuracy, showing deviations of only 1% and 8%, respectively, when compared to coefficients calculated from experimental adsorption data. The highest deviation of 84% from the experimental Henry coefficient is observed for Fe-MOF-74. This is clearly reflected in the disparity of the simulated isotherm shape to the experimental data, particularly in the low-pressure region, as illustrated in Fig. S1d.

MOF-74	$K_{\mathrm{H,sim}}$ [mol kg^{-1} Pa^{-1}]	$K_{\mathrm{H,exp}}$ [mol kg^{-1} Pa^{-1}]
Ni-	$0.50_{0.03}$	0.46
Cu-	$0.000403_{3\cdot10^{-6}}$	0.0004
Co-	$0.03_{0.01}$	0.0205
Fe-	$0.0029_{2\cdot10^{-4}}$	0.0183
Mn-	$0.00275_{9\cdot10^{-5}}$	0.0043
Zn-	$0.00200_{4\cdot10^{-5}}$	-

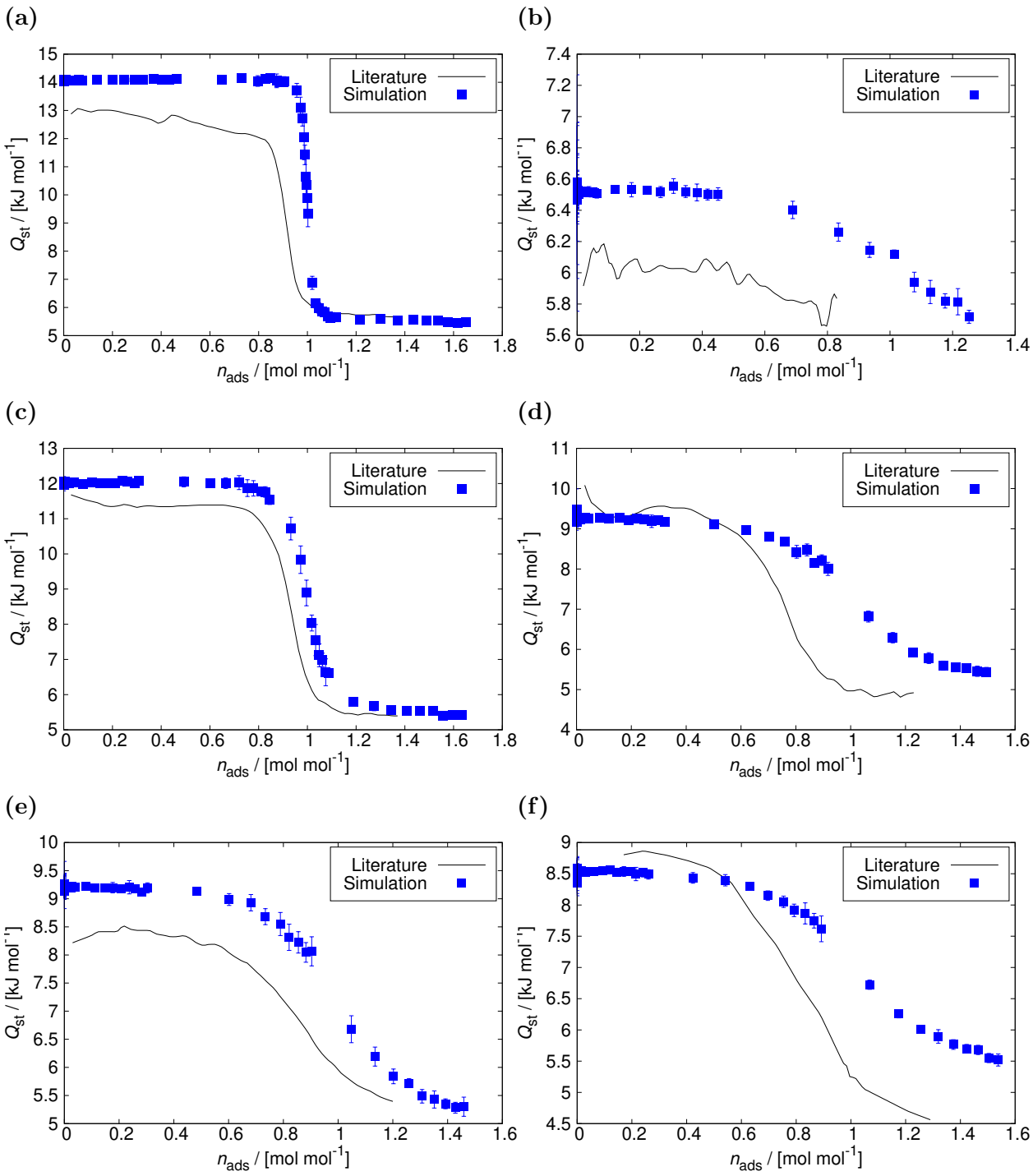

Fig. S2. Heat of adsorption of H_2 computed from GCMC simulations using the RASPA software package[18,19] at 77 K, and 10^{-5} - 10^{2} kPa in: (a) Ni-MOF-74, (b) Cu-MOF-74, (c) Co-MOF-74, (d) Fe-MOF-74, (e) Mn-MOF-74, and (f) Zn-MOF-74. The heat of adsorption results computed from the adjusted force field are represented by blue data points, and the experimental data from literature[21] by solid black lines. The force field agrees well with the experimental values, with a slight shift towards a higher uptake observed for Fe-MOF-74.

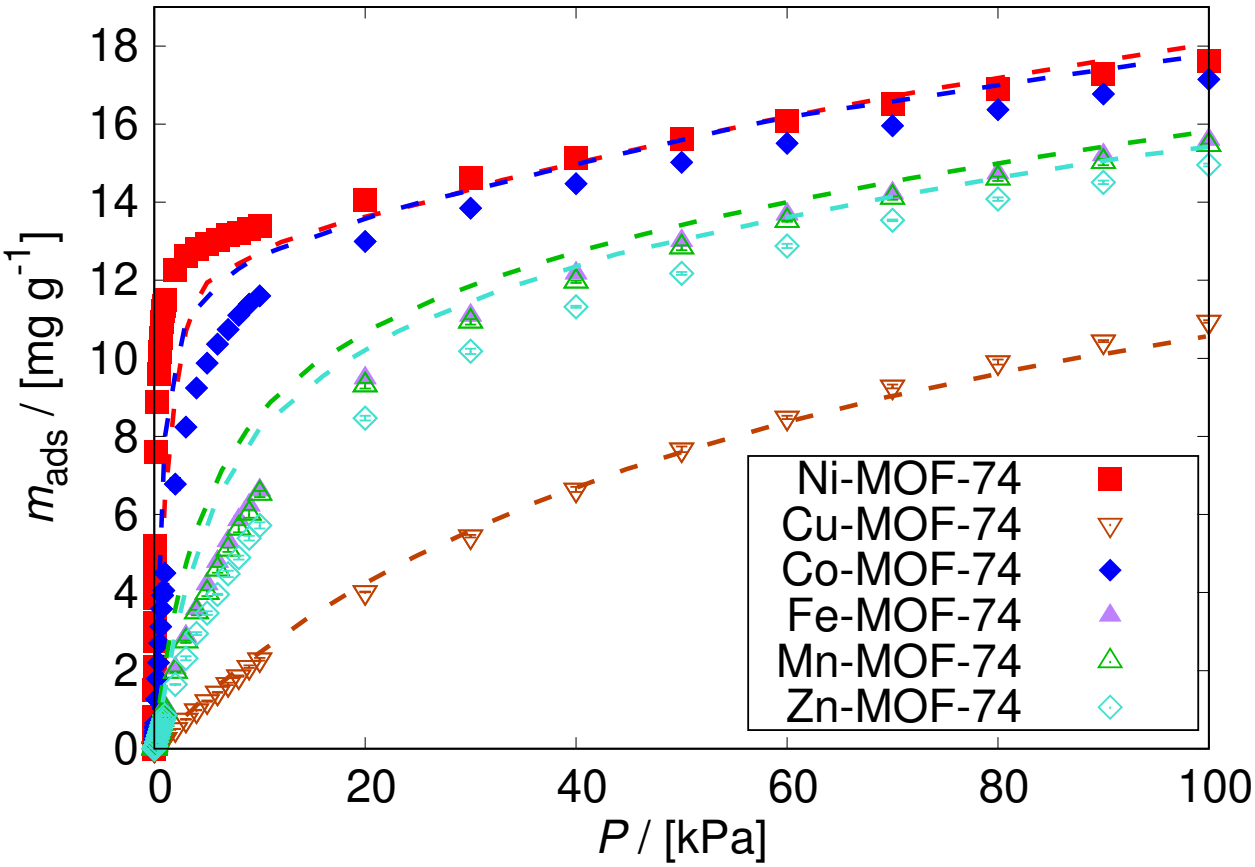

Fig. S3. Adsorption isotherms of H_2 computed from GCMC simulations using the RASPA software package[18,19] at 87 K, and 10^{-5} - 10^{2} kPa in M-MOF-74 (M = Ni, Cu, Co, Fe, Mn, Zn). The adsorption results computed from the adjusted force field are represented by data points, and the experimental data[21,24,25] by dashed lines with corresponding colors. The error bars are smaller than the size of the symbols. The simulations reproduce the experimental values, showing the temperature transferability of the force field from 77 K to 87 K.

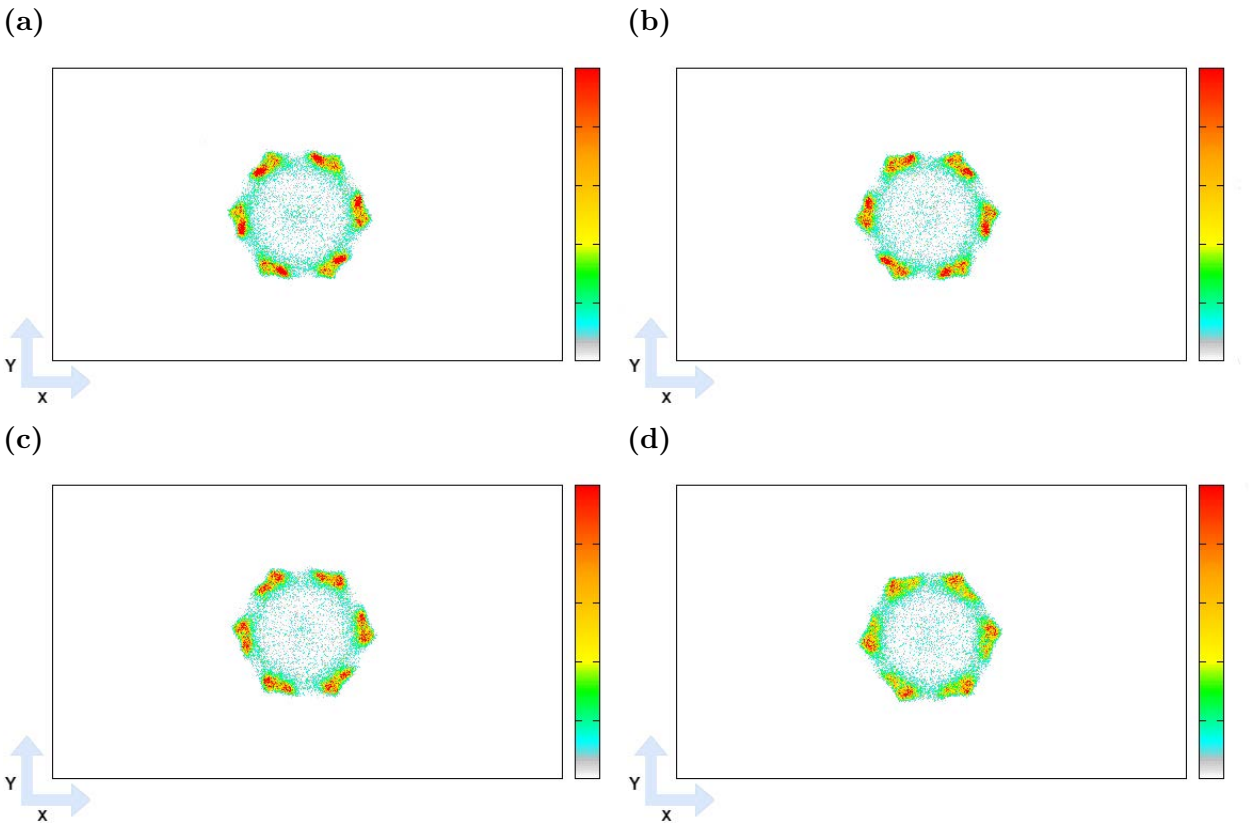

Fig. S4. The distribution of the CO_2 molecules analyzed using density profiles from GCMC simulations at 298 K, 100 kPa in: (a) Co-MOF-74, (b) Fe-MOF-74, (c) Mn-MOF-74, (d) Zn-MOF-74. The center of mass of the molecules that are adsorbed was projected onto the XY plane. The color gradation of the scales relates to the most and least populated regions of the structure, which is relative in each case. The color scale is shown as a reference of the loading. The preferential sites of CO_2 (colored red) in all M-MOF-74 are at the open-metal centers.

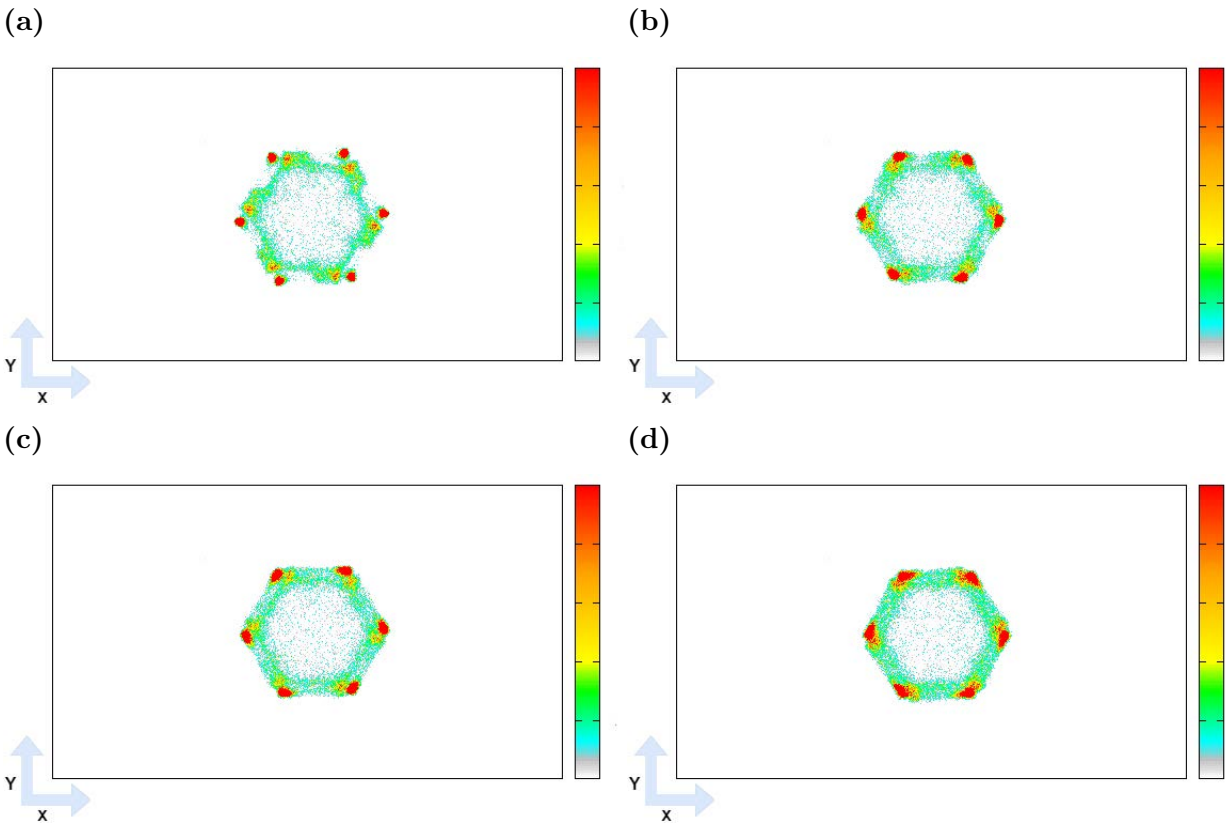

Fig. S5. The distribution of the H_2 molecules analyzed using density profiles from GCMC simulations at 77 K, 100 kPa in: (a) Co-MOF-74, (b) Fe-MOF-74, (c) Mn-MOF-74, (d) Zn-MOF-74. The center of mass of the molecules that are adsorbed was projected onto the XY plane. The color gradation of the scales relates to the most and least populated regions of the structure, which is relative in each case. The color scale is shown as a reference of the molecules loading. The preferential sites of H_2 (colored red) in all M-MOF-74 are at the open-metal centers.

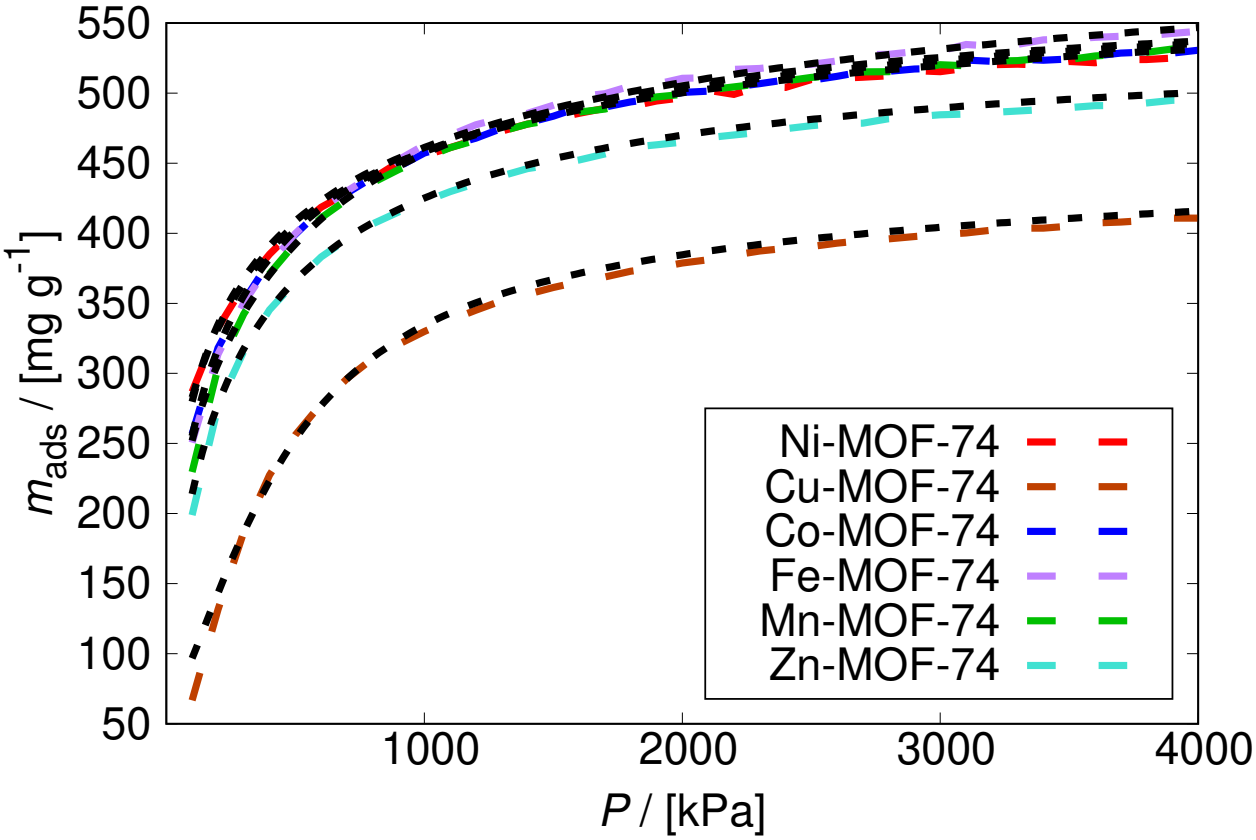

Fig. S6. The prediction of CO_2/H_2 gas mixture adsorption using IAST[26] obtained from RUPTURA[20] for $y_{CO_2} = 0.5$ in M-MOF-74 (M = Ni, Cu, Co, Fe, Mn, Zn) at 298.15 K, and 100 - 4000 kPa, compared to the GCMC simulations from RASPA.[18,19] The adsorption loading for CO_2 computed from GCMC simulations of the binary mixture is represented by data points, and the IAST prediction by black, dashed lines. The loading for H_2 was omitted as it is lower than 1 mg g^{-1} of H_2 in all the M-MOF-74 frameworks. The results obtained from IAST mixture prediction using RUPTURA agree well with the multicomponent GCMC simulations, meaning that the validation of the breakthrough curves was successful.

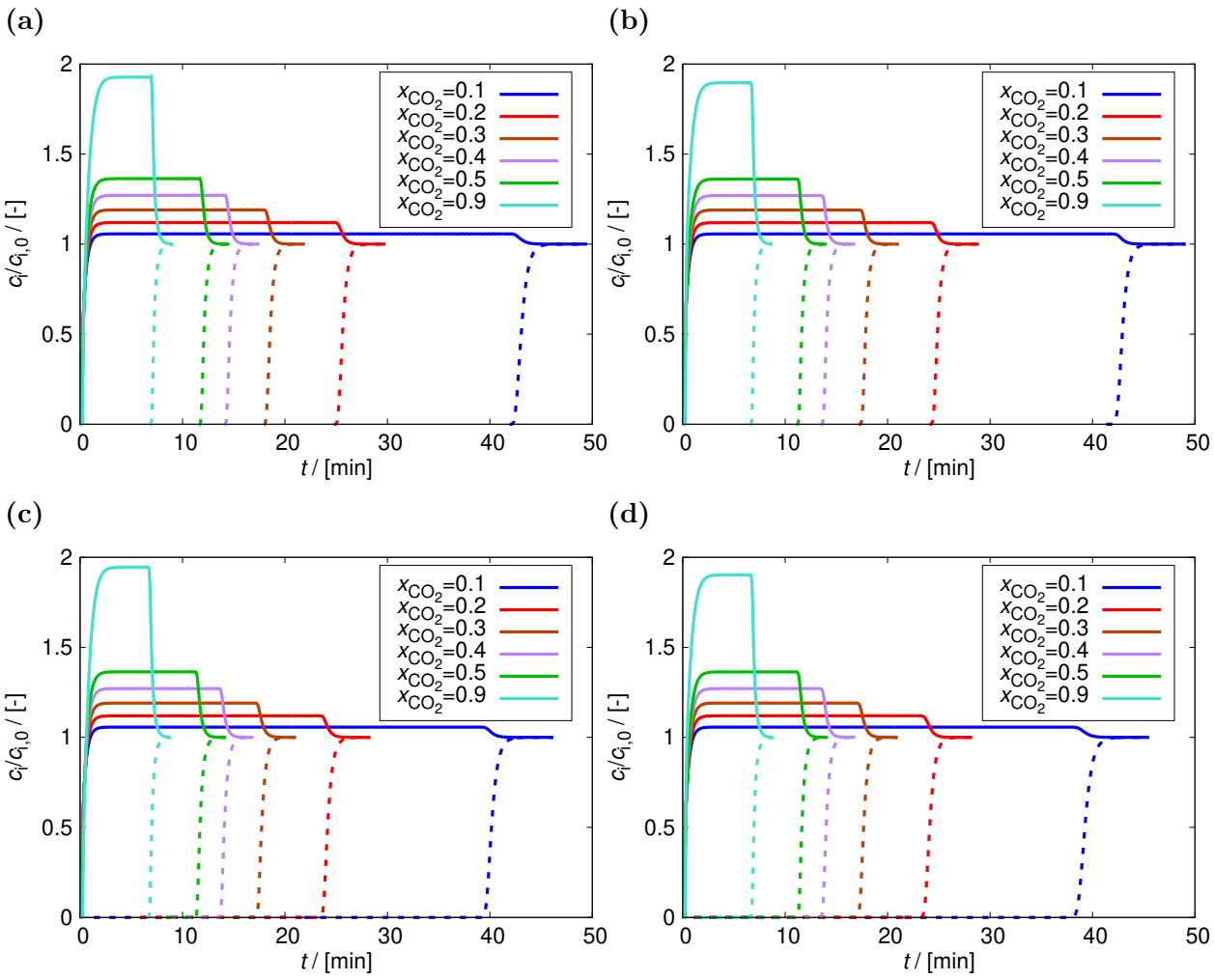

Fig. S7. Breakthrough curves computed from RUPTURA[20] for the separation of CO_2/H_2 mixtures in fixed-bed adsorbers at CO_2 feed mole fractions of y_{CO_2} = 0.1, 0.2, 0.3, 0.4, 0.5, 0.9, using: (a) Co-MOF-74, (b) Fe-MOF-74, (c) Mn-MOF-74, (d) Zn-MOF-74. The breakthrough curves of CO_2 are represented by dashed lines, and the breakthrough curves of H_2 by solid lines. The initial conditions are specified as: temperature T=298 K, total pressure p_T = 2.5 MPa, packed bed void fraction ε_B = 0.4, interstitial gas velocity entering the packed bed v = 0.006791 m s^{-1}, length of packed bed adsorber L = 0.065 m, axial dispersion is neglected, and isothermal conditions are assumed.

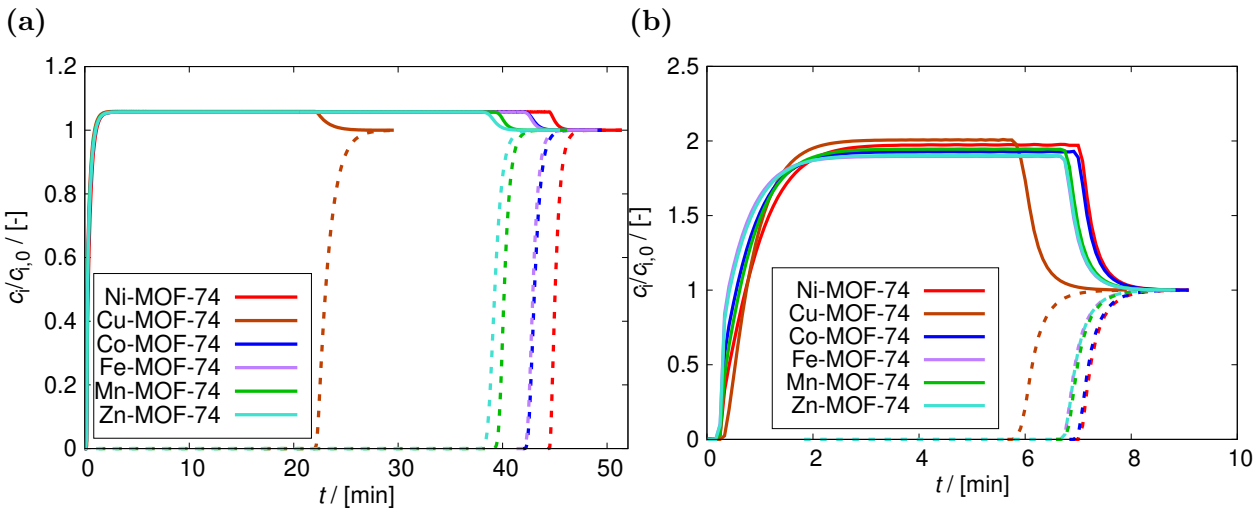

Fig. S8. Breakthrough curves computed from RUPTURA[20] for the separation of CO_2/H_2 mixtures in fixed-bed adsorbers using M-MOF-74 (M = Ni, Cu, Co, Fe, Mn, Zn) at CO_2 feed mole fractions of: (a) $y_{CO_2} = 0.1$, (b) $y_{CO_2} = 0.9$. The breakthrough curves of CO_2 are represented by dashed lines, and the breakthrough curves of H_2 by solid lines. The initial conditions are specified as: temperature T=298 K, total pressure $p_T = 2.5$ MPa, packed bed void fraction $\varepsilon_B = 0.4$, interstitial gas velocity entering the packed bed $v = 0.006791$ m s^{-1}, length of packed bed adsorber $L = 0.065$ m, axial dispersion is neglected, and isothermal conditions are assumed.

- Ni-MOF-74.cif

```
data_Ni-MOF-74-cCO2

_audit_creation_method RASPA-1.0
_audit_creation_date 2019-12-13
_audit_author_name 'Jose Manuel Vicent-Luna'

_cell_length_a    25.7856
_cell_length_b    25.7856
_cell_length_c    6.7701
_cell_angle_alpha 90
_cell_angle_beta  90
_cell_angle_gamma 120
_cell_volume      15593.4
_symmetry_cell_setting          trigonal
_symmetry_space_group_name_Hall '-R 3'
_symmetry_space_group_name_H-M  'R -3'
_symmetry_Int_Tables_number     148

loop_
_symmetry_equiv_pos_as_xyz
 'x,y,z'
 '-y,x-y,z'
 '-x+y,-x,z'
 '-x,-y,-z'
 'y,-x+y,-z'
 'x-y,x,-z'
 'x+2/3,y+1/3,z+1/3'
 '-y+2/3,x-y+1/3,z+1/3'
 '-x+y+2/3,-x+1/3,z+1/3'
 '-x+2/3,-y+1/3,-z+1/3'
 'y+2/3,-x+y+1/3,-z+1/3'
 'x-y+2/3,x+1/3,-z+1/3'
 'x+1/3,y+2/3,z+2/3'
 '-y+1/3,x-y+2/3,z+2/3'
 '-x+y+1/3,-x+2/3,z+2/3'
 '-x+1/3,-y+2/3,-z+2/3'
 'y+1/3,-x+y+2/3,-z+2/3'
 'x-y+1/3,x+2/3,-z+2/3'

loop_
_atom_site_label
_atom_site_type_symbol
_atom_site_fract_x
_atom_site_fract_y
_atom_site_fract_z
_atom_site_charge
Ni       Ni     0.018170     0.713530     0.188130     1.55
C1       C      0.260070     0.914730     0.085340     0.603
C2       C      0.212570     0.875030     0.960330    -0.275
C3       C      0.123270     0.775530     0.910330     0.275
C4       C      0.168170     0.816730     0.035340    -0.086
O1       O      0.262870     0.899130     0.265340    -0.63
O2       O      0.300270     0.964230     0.020330    -0.815
O3       O      0.082870     0.721130     0.979330    -0.702
H        H      0.170670     0.804330     0.193330     0.08
```

- Cu-MOF-74.cif

```
data_Cu-MOF-74-cCO2

_audit_creation_method RASPA-1.0
_audit_creation_date 2019-12-13
_audit_author_name 'Jose Manuel Vicent-Luna'

_cell_length_a    25.9972
_cell_length_b    25.9972
_cell_length_c    6.2587
_cell_angle_alpha 90
_cell_angle_beta  90
_cell_angle_gamma 120
_cell_volume      14653

_symmetry_cell_setting          trigonal
_symmetry_space_group_name_Hall '-R 3'
_symmetry_space_group_name_H-M  'R -3'
_symmetry_Int_Tables_number     148

loop_
_symmetry_equiv_pos_as_xyz
 'x,y,z'
 '-y,x-y,z'
 '-x+y,-x,z'
 '-x,-y,-z'
 'y,-x+y,-z'
 'x-y,x,-z'
 'x+2/3,y+1/3,z+1/3'
 '-y+2/3,x-y+1/3,z+1/3'
 '-x+y+2/3,-x+1/3,z+1/3'
 '-x+2/3,-y+1/3,-z+1/3'
 'y+2/3,-x+y+1/3,-z+1/3'
 'x-y+2/3,x+1/3,-z+1/3'
 'x+1/3,y+2/3,z+2/3'
 '-y+1/3,x-y+2/3,z+2/3'
 '-x+y+1/3,-x+2/3,z+2/3'
 '-x+1/3,-y+2/3,-z+2/3'
 'y+1/3,-x+y+2/3,-z+2/3'
 'x-y+1/3,x+2/3,-z+2/3'

loop_
_atom_site_label
_atom_site_type_symbol
_atom_site_fract_x
_atom_site_fract_y
_atom_site_fract_z
_atom_site_charge
Cu       Cu     0.290950     0.015230     0.346670     0.834
C1       C      0.169800     0.816900     0.538500    -0.076
C2       C      0.257700     0.913900     0.625600     0.345
C3       C      0.209600     0.890500     0.255200     0.156
C4       C      0.212100     0.872700     0.466900    -0.139
O1       O      0.250190     0.943270     0.168700    -0.394
O2       O      0.284800     0.969230     0.598900    -0.431
O3       O      0.266220     0.890810     0.789000    -0.368
H        H      0.172500     0.806100     0.681200     0.073
```

- Co-MOF-74.cif

```
data_Co-MOF-74-cCO2

_audit_creation_method RASPA-1.0
_audit_creation_date 2019-12-13
_audit_author_name 'Jose Manuel Vicent-Luna'

_cell_length_a    25.885
_cell_length_b    25.885
_cell_length_c    6.8058
_cell_angle_alpha 90
_cell_angle_beta  90
_cell_angle_gamma 120
_cell_volume      15796.7

_symmetry_cell_setting          trigonal
_symmetry_space_group_name_Hall '-R 3'
_symmetry_space_group_name_H-M  'R -3'
_symmetry_Int_Tables_number     148

loop_
_symmetry_equiv_pos_as_xyz
 'x,y,z'
 '-y,x-y,z'
 '-x+y,-x,z'
 '-x,-y,-z'
 'y,-x+y,-z'
 'x-y,x,-z'
 'x+2/3,y+1/3,z+1/3'
 '-y+2/3,x-y+1/3,z+1/3'
 '-x+y+2/3,-x+1/3,z+1/3'
 '-x+2/3,-y+1/3,-z+1/3'
 'y+2/3,-x+y+1/3,-z+1/3'
 'x-y+2/3,x+1/3,-z+1/3'
 'x+1/3,y+2/3,z+2/3'
 '-y+1/3,x-y+2/3,z+2/3'
 '-x+y+1/3,-x+2/3,z+2/3'
 '-x+1/3,-y+2/3,-z+2/3'
 'y+1/3,-x+y+2/3,-z+2/3'
 'x-y+1/3,x+2/3,-z+2/3'

loop_
_atom_site_label
_atom_site_type_symbol
_atom_site_fract_x
_atom_site_fract_y
_atom_site_fract_z
_atom_site_charge
Co       Co     0.048500     0.362110     0.975420     1.335
C1       C      0.086900     0.347400     0.594700     0.485
C2       C      0.126400     0.339400     0.453700    -0.207
C3       C      0.011100     0.455300     0.923700     0.245
C4       C      0.016900     0.501800     0.808190    -0.125
O1       O      0.104200     0.365300     0.766600    -0.544
O2       O      0.022100     0.414400     0.838700    -0.611
O3       O      0.329130     0.032570     0.865760    -0.673
H        H      0.028400     0.503700     0.677800     0.095
```

- Fe-MOF-74.cif

```
data_Fe-MOF-74-cCO2

_audit_creation_method RASPA-1.0
_audit_creation_date 2019-12-13
_audit_author_name 'Jose Manuel Vicent-Luna'

_cell_length_a    26.1627
_cell_length_b    26.1627
_cell_length_c    6.8422
_cell_angle_alpha 90
_cell_angle_beta  90
_cell_angle_gamma 120
_cell_volume      16223.8

_symmetry_cell_setting          trigonal
_symmetry_space_group_name_Hall '-R 3'
_symmetry_space_group_name_H-M  'R -3'
_symmetry_Int_Tables_number     148

loop_
_symmetry_equiv_pos_as_xyz
 'x,y,z'
 '-y,x-y,z'
 '-x+y,-x,z'
 '-x,-y,-z'
 'y,-x+y,-z'
 'x-y,x,-z'
 'x+2/3,y+1/3,z+1/3'
 '-y+2/3,x-y+1/3,z+1/3'
 '-x+y+2/3,-x+1/3,z+1/3'
 '-x+2/3,-y+1/3,-z+1/3'
 'y+2/3,-x+y+1/3,-z+1/3'
 'x-y+2/3,x+1/3,-z+1/3'
 'x+1/3,y+2/3,z+2/3'
 '-y+1/3,x-y+2/3,z+2/3'
 '-x+y+1/3,-x+2/3,z+2/3'
 '-x+1/3,-y+2/3,-z+2/3'
 'y+1/3,-x+y+2/3,-z+2/3'
 'x-y+1/3,x+2/3,-z+2/3'

loop_
_atom_site_label
_atom_site_type_symbol
_atom_site_fract_x
_atom_site_fract_y
_atom_site_fract_z
_atom_site_charge
Fe       Fe     0.382300     0.350970     0.139570     1.226
C1       C      0.317610     0.245000     0.427190     0.356
C2       C      0.330280     0.205750     0.293830    -0.148
C3       C      0.343180     0.222470     0.089460     0.175
C4       C      0.352650     0.180570     0.965880    -0.088
O1       O      0.327500     0.294890     0.363950    -0.602
O2       O      0.297710     0.219750     0.598130    -0.439
O3       O      0.356720     0.274650     0.004040    -0.561
H        H      0.361740     0.190690     0.834200     0.081
```

- Mn-MOF-74.cif

```
data_Mn-MOF-74-cCO2

_audit_creation_method RASPA-1.0
_audit_creation_date 2019-12-13
_audit_author_name 'Jose Manuel Vicent-Luna'

_cell_length_a    25.7824
_cell_length_b    25.7824
_cell_length_c    6.9126
_cell_angle_alpha 90
_cell_angle_beta  90
_cell_angle_gamma 120
_cell_volume      15917.6

_symmetry_cell_setting          trigonal
_symmetry_space_group_name_Hall '-R 3'
_symmetry_space_group_name_H-M  'R -3'
_symmetry_Int_Tables_number     148

loop_
_symmetry_equiv_pos_as_xyz
 'x,y,z'
 '-y,x-y,z'
 '-x+y,-x,z'
 '-x,-y,-z'
 'y,-x+y,-z'
 'x-y,x,-z'
 'x+2/3,y+1/3,z+1/3'
 '-y+2/3,x-y+1/3,z+1/3'
 '-x+y+2/3,-x+1/3,z+1/3'
 '-x+2/3,-y+1/3,-z+1/3'
 'y+2/3,-x+y+1/3,-z+1/3'
 'x-y+2/3,x+1/3,-z+1/3'
 'x+1/3,y+2/3,z+2/3'
 '-y+1/3,x-y+2/3,z+2/3'
 '-x+y+1/3,-x+2/3,z+2/3'
 '-x+1/3,-y+2/3,-z+2/3'
 'y+1/3,-x+y+2/3,-z+2/3'
 'x-y+1/3,x+2/3,-z+2/3'

loop_
_atom_site_label
_atom_site_type_symbol
_atom_site_fract_x
_atom_site_fract_y
_atom_site_fract_z
_atom_site_charge
Mn       Mn     0.639720     0.690220     0.484690     1.161
C1       C      0.926810     0.244410     0.427820     0.368
C2       C      0.879080     0.206580     0.291510    -0.175
C3       C      0.210810     0.890160     0.763230     0.175
C4       C      0.165210     0.849500     0.643290    -0.064
O1       O      0.970970     0.293680     0.363200    -0.548
O2       O      0.924140     0.227920     0.602680    -0.443
O3       O      0.250820     0.943470     0.687320    -0.522
H        H      0.164180     0.862120     0.492850     0.048
```

- Zn-MOF-74.cif

```
data_Zn-MOF-74-cCO2

_audit_creation_method RASPA-1.0
_audit_creation_date 2019-12-13
_audit_author_name 'Jose Manuel Vicent-Luna'

_cell_length_a    25.9322
_cell_length_b    25.9322
_cell_length_c    6.8365
_cell_angle_alpha 90
_cell_angle_beta  90
_cell_angle_gamma 120
_cell_volume      15925.9

_symmetry_cell_setting          trigonal
_symmetry_space_group_name_Hall '-R 3'
_symmetry_space_group_name_H-M  'R -3'
_symmetry_Int_Tables_number     148

loop_
_symmetry_equiv_pos_as_xyz
 'x,y,z'
 '-y,x-y,z'
 '-x+y,-x,z'
 '-x,-y,-z'
 'y,-x+y,-z'
 'x-y,x,-z'
 'x+2/3,y+1/3,z+1/3'
 '-y+2/3,x-y+1/3,z+1/3'
 '-x+y+2/3,-x+1/3,z+1/3'
 '-x+2/3,-y+1/3,-z+1/3'
 'y+2/3,-x+y+1/3,-z+1/3'
 'x-y+2/3,x+1/3,-z+1/3'
 'x+1/3,y+2/3,z+2/3'
 '-y+1/3,x-y+2/3,z+2/3'
 '-x+y+1/3,-x+2/3,z+2/3'
 '-x+1/3,-y+2/3,-z+2/3'
 'y+1/3,-x+y+2/3,-z+2/3'
 'x-y+1/3,x+2/3,-z+2/3'

loop_
_atom_site_label
_atom_site_type_symbol
_atom_site_fract_x
_atom_site_fract_y
_atom_site_fract_z
_atom_site_charge
Zn       Zn     0.280080     0.982240     0.687100     1.006
C1       C      0.350670     0.087270     0.411730     0.343
C2       C      0.339610     0.125890     0.548730    -0.155
C3       C      0.322980     0.111220     0.747630     0.161
C4       C      0.317830     0.153290     0.859230    -0.083
O1       O      0.345470     0.039270     0.476730    -0.479
O2       O      0.365000     0.104470     0.237730    -0.393
O3       O      0.311450     0.059840     0.834040    -0.464
H        H      0.307470     0.144730     0.993330     0.064
```

References

(1) Dietzel, P. D. C.; Panella, B.; Hirscher, M.; Blom, R.; Fjellvåg, H. Hydrogen Adsorption in a Nickel Based Coordination Polymer with Open Metal Sites in the Cylindrical Cavities of the Desolvated Framework. *Chemical Communications* **2006**, *9*, 959–961.

(2) Sanz, R.; Martínez, F.; Orcajo, G.; Wojtas, L.; Briones, D. Synthesis of a Honeycomb-Like Cu-Based Metal–Organic Framework and Its Carbon Dioxide Adsorption Behaviour. *Dalton Transactions* **2013**, *42*, 2392–2398.

(3) Dietzel, P. D.; Morita, Y.; Blom, R.; Fjellvåg, H. An In Situ High-Temperature Single-Crystal Investigation of a Dehydrated Metal–Organic Framework Compound and Field-Induced Magnetization of One-Dimensional Metal–Oxygen Chains. *Angewandte Chemie* **2005**, *117*, 6512–6516.

(4) Bhattacharjee, S.; Choi, J.-S.; Yang, S.-T.; Choi, S. B.; Kim, J.; Ahn, W.-S. Solvothermal Synthesis of Fe-MOF-74 and Its Catalytic Properties in Phenol Hydroxylation. *Journal of Nanoscience and Nanotechnology* **2010**, *10*, 135–141.

(5) Zhou, W.; Wu, H.; Yildirim, T. Enhanced H_2 Adsorption in Isostructural Metal–Organic Frameworks with Open Metal Sites: Strong Dependence of the Binding Strength on Metal Ions. *Journal of the American Chemical Society* **2008**, *130*, 15268–15269.

(6) Rosi, N. L.; Kim, J.; Eddaoudi, M.; Chen, B.; O'Keeffe, M.; Yaghi, O. M. Rod Packings and Metal-Organic Frameworks Constructed from Rod-Shaped Secondary Building Units. *Journal of the American Chemical Society* **2005**, *127*, 1504–1518.

(7) Mayo, S. L.; Olafson, B. D.; Goddard, W. A. DREIDING: a Generic Force Field for Molecular Simulations. *Journal of Physical Chemistry* **1990**, *94*, 8897–8909.

(8) Rappe, A. K.; Casewit, C. J.; Colwell, K. S.; Goddard, W. A.; Skiff, W. M. UFF, a Full Periodic Table Force Field for Molecular Mechanics and Molecular Dynamics Simulations. *Journal of the American Chemical Society* **1992**, *114*, 10024–10035.

(9) Harris, J. G.; Yung, K. H. Carbon Dioxide's Liquid-Vapor Coexistence Curve And Critical Properties as Predicted by a Simple Molecular Model. *Journal of Physical Chemistry* **1995**, *99*, 12021–12024.

(10) García-Sánchez, A.; Ania, C. O.; Parra, J. B.; Dubbeldam, D.; Vlugt, T. J. H.; Krishna, R.; Calero, S. Transferable Force Field for Carbon Dioxide Adsorption in Zeolites. *Journal of Physical Chemistry C* **2009**, *113*, 8814–8820.

(11) Darkrim, F.; Levesque, D. Monte Carlo Simulations of Hydrogen Adsorption in Single-Walled Carbon Nanotubes. *Journal of Chemical Physics* **1998**, *109*, 4981–4984.

(12) Allen, M. P.; Tildesley, D. J. *Computer Simulation of Liquids*, 2nd ed.; Oxford University Press: Oxford, UK, 2017.

(13) Wilmer, C. E.; Snurr, R. Q. Towards Rapid Computational Screening of Metal-Organic Frameworks for Carbon Dioxide Capture: Calculation of Framework Charges via Charge Equilibration. *Chemical Engineering Journal* **2011**, *171*, 775–781.

(14) Wilmer, C. E.; Kim, K. C.; Snurr, R. Q. An Extended Charge Equilibration Method. *Journal of Physical Chemistry Letters* **2012**, *3*, 2506–2511.

(15) Queen, W. L.; Hudson, M. R.; Bloch, E. D.; Mason, J. A.; Gonzalez, M. I.; Lee, J. S.; Gygi, D.; Howe, J. D.; Lee, K.; Darwish, T. A., et al. Comprehensive Study of Carbon Dioxide Adsorption in the Metal–Organic Frameworks M_2 (dobdc)(M= Mg, Mn, Fe, Co, Ni, Cu, Zn). *Chemical Science* **2014**, *5*, 4569–4581.

(16) Luna-Triguero, A.; Vicent-Luna, J. M.; Madero-Castro, R. M.; Gómez-Álvarez, P.; Calero, S. Acetylene Storage and Separation Using Metal–Organic Frameworks with Open Metal Sites. *ACS Applied Materials & Interfaces* **2019**, *11*, 31499–31507.

(17) Langmuir, I. The Adsorption of Gases on Plane Surfaces of Glass, Mica and Platinum. *Journal of the American Chemical society* **1918**, *40*, 1361–1403.

(18) Dubbeldam, D.; Calero, S.; Ellis, D. E.; Snurr, R. Q. RASPA: Molecular Simulation Software for Adsorption and Diffusion in Flexible Nanoporous Materials. *Molecular Simulation* **2016**, *42*, 81–101.

(19) Dubbeldam, D.; Torres-Knoop, A.; Walton, K. S. On the Inner Workings of Monte Carlo Codes. *Molecular Simulation* **2013**, *39*, 1253–1292.

(20) Sharma, S.; Balestra, S. R. G.; Baur, R.; Agarwal, U.; Zuidema, E.; Rigutto, M. S.; Calero, S.; Vlugt, T. J. H.; Dubbeldam, D. RUPTURA: Simulation Code for Breakthrough, Ideal Adsorption Solution Theory Computations, and Fitting of Isotherm Models. *Molecular Simulation* **2023**, *49*, 893–953.

(21) Rosnes, M. H.; Opitz, M.; Frontzek, M.; Lohstroh, W.; Embs, J. P.; Georgiev, P. A.; Dietzel, P. D. Intriguing Differences in Hydrogen Adsorption in CPO-27 Materials Induced by Metal Substitution. *Journal of Materials Chemistry A* **2015**, *3*, 4827–4839.

(22) Frenkel, D.; Smit, B. *Understanding Molecular Simulation: From Algorithms to Applications*, 3rd ed.; Elsevier, 2023.

(23) Atkins, P.; De Paula, J.; Keeler, J. *Atkins' Physical Chemistry*, 12th ed.; Oxford University Press, 2023.

(24) Dietzel, P. D. C.; Georgiev, P. A.; Eckert, J.; Blom, R.; Strässle, T.; Unruh, T. Interaction of Hydrogen with Accessible Metal Sites in the Metal-Organic Frameworks M_2(dhtp) (CPO-27-M; M = Ni, Co, Mg). *Chemical Communications* **2010**, *46*, 4962–4964.

(25) Rowsell, J. L. C.; Yaghi, O. M. Effects of Functionalization, Catenation, and Variation of the Metal Oxide and Organic Linking Units on the Low-Pressure Hydrogen Adsorption Properties of Metal–Organic Frameworks. *Journal of the American Chemical Society* **2006**, *128*, 1304–1315.

(26) Myers, A. L.; Prausnitz, J. M. Thermodynamics of Mixed-Gas Adsorption. *AIChE Journal* **1965**, *11*, 121–127.